

Probe nuclear structure using the anisotropic flow at the Large Hadron Collider

Zhiyong Lu¹, Mingrui Zhao^{1,2}, Jiangyong Jia^{3,4}, and You Zhou^{2,a}

¹ China Institute of Atomic Energy, China

² Niels Bohr Institute, University of Copenhagen, Denmark

³ Department of Chemistry, Stony Brook University, USA

⁴ Physics Department, Brookhaven National Laboratory, Upton, NY 11976, USA

Abstract. Recent studies have shown that the shape and radial profile of the colliding nuclei have strong influences on the initial condition of the heavy ion collisions and the subsequent development of the anisotropic flow. Using A Multi-Phase Transport model (AMPT) model, we investigated the impact of nuclear quadrupole deformation β_2 and nuclear diffuseness a_0 of ^{129}Xe on various of flow observables in Xe–Xe collisions at $\sqrt{s_{NN}} = 5.44$ TeV. We found that β_2 has a strong influence on central collisions while a_0 mostly influences the mid-central collisions. The relative change of flow observables induced by a change in β_2 and a_0 are also found to be insensitive to the values of parameters controlling the strength of the interaction among final state particles. Our study demonstrates the potential for constraining the initial condition of heavy ion collisions using future system scans at the LHC.

1 Introduction

Ultra-relativistic heavy-ion collisions conducted at both the Relativistic Heavy-Ion Collider (RHIC) and the Large Hadron Collider (LHC) provide a pivotal platform for the comprehensive study of Quantum Chromodynamics (QCD) across both perturbative and nonperturbative regimes. These collisions afford the remarkable opportunity to recreate a novel state of matter, quark-gluon plasma (QGP), characterized by extreme temperatures and densities in the early stages of high-energy heavy-ion interactions. Over the past two decades, a dedicated endeavor has been directed towards extracting precise insights into the properties and the dynamic evolution of QGP [1–11]. Anisotropic flow, which quantifies the anisotropic expansion of the produced particles, has been a powerful tool for QGP studies [5–11]. It is characterized by the Fourier coefficients v_n of the azimuthal particle distribution [12]:

$$f(\varphi) = \frac{1}{2\pi} \left[1 + 2 \sum_{n=1}^{\infty} v_n \cos[n(\varphi - \Psi_n)] \right] \quad (1)$$

where φ is the azimuthal angle of the final particles, Ψ_n is the n_{th} -order flow symmetry plane, and v_n is called flow coefficient. From Eq(1), the flow coefficient v_n can be

^a e-mail: you.zhou@cern.ch

defined as:

$$v_n = \langle \cos[n(\varphi - \Psi_n)] \rangle. \quad (2)$$

Here, the angular bracket $\langle \rangle$ denotes the average over all particles in one event. The v_n and flow angle Ψ_n are the magnitude (amplitude) and angle (orientation) of the flow vector, defined as:

$$V_n \equiv v_n e^{in\Psi_n} \quad (3)$$

Systematic measurements on v_n , event-by-event fluctuations of v_n , and correlations of different flow coefficients v_n, v_m, v_k have been previously reported in Refs. [13–17]. By performing the Bayesian fit on the extensive flow data, critical information on the temperature dependence of shear and bulk viscosity over entropy density ratios of the QGP, $\eta/s(T)$ and $\zeta/s(T)$, can be extracted [18–21].

In addition, the flow measurements give direct access to the event-averaged initial-state shape of the nuclear overlap region and their event-by-event fluctuations. For typical heavy-ion collisions, the nuclear density profile in the initial-state can be described by Woods-Saxon distribution:

$$\rho(r, \theta, \phi) = \frac{\rho_0}{1 + e^{[r - R(\theta, \phi)]/a_0}},$$

$$R(\theta, \phi) = R_0(1 + \beta_2[\cos \gamma Y_{2,0} + \sin \gamma Y_{2,2}] + \beta_3 \sum_{m=-3}^3 \alpha_{3,m} Y_{3,m} + \beta_4 \sum_{m=-4}^4 \alpha_{4,m} Y_{4,m}) \quad (4)$$

where a_0 denotes the nuclear diffuseness, while R_0 represents the half-width radius. The nuclear surface, denoted as $R(\theta, \phi)$, is expanded in terms of spherical harmonics $Y_{n,m}$, where we retain terms up to $n = 4$ as expressed in the Eq. (4). Furthermore, β_2, β_3 , and β_4 stand for the quadrupole, octupole, and hexadecapole deformation parameters, respectively. The parameter γ characterizes the triaxial shape, depicting any imbalance present within the axes of the spheroid. Analogous to γ , $\alpha_{3,m}$ and $\alpha_{4,m}$ describe the inequality of axes and satisfy the normalization condition.

In recent years, various observables have been investigated for their sensitivities to nuclear structure parameters in heavy-ion collisions [22–29]. As mentioned above, the anisotropic flow reflects the initial spatial anisotropies in the overlap region of the colliding nucleus. Thus, it serves as an ideal probe of initial conditions and can be utilized for the nuclear structure study. The flow coefficient v_n has been found to be sensitive to the deformation, characterized by deformation parameters β_n , in ^{96}Ru – ^{96}Ru , ^{96}Zr – ^{96}Zr , ^{238}U – ^{238}U , ^{197}Au – ^{197}Au collisions [22–26]. Beyond v_n , the spotlight extends to multi-particle cumulants of v_n and nonlinear flow, underlining their potential for discerning the parameters β_n , a_0 , and R_0 [25–27]. Moreover, the mean transverse momentum of the produced charged hadrons, denoted as $[p_T]$, which reflects the initial overlap region’s size, is a valuable probe for exploring neutron skin thickness and nuclear deformation [28]. The fluctuations of v_n and $[p_T]$, as well as the correlations between them, quantified by Pearson correlation coefficient (PCC) and denoted as $\rho(v_n^2, [p_T])$, emerge as a nuanced avenue for constraining deformation parameters β_n and the triaxial parameter γ [29].

Almost all these studies are conducted within the RHIC energies (GeV energy scale), while a similar study at the LHC energies ranges (TeV energy scale) is still lacking at the moment. In particular, ^{129}Xe is the nucleus believed to have quadrupole and triaxial deformation [30], determined from low-energy nuclear theory and experiments [31–36]. Nevertheless, only very few selected flow observables, such as $v_n\{2\}$ and $\rho(v_n^2, [p_T])$, have been studied so far [37, 38]. The realm of systematic investigations targeting more intricate flow observables, based on multi-particle correlations

in the final state that potentially tie into the many-body interactions within nuclei prior to collisions, are currently unavailable at the LHC.

This paper will present comprehensive investigations of the nuclear structure using various flow observables, such as flow coefficients, flow fluctuations, correlations between flow coefficients, and nonlinear flow modes, based on the AMPT model simulations. We also study how the final state effects influence these flow observables to ensure that the nuclear parameters can be constrained without being biased by the final state effects.

2 A Multi-Phase Transport Model

A Multi-Phase Transport (AMPT) Model [39] holds widespread application in the realm of ultra-relativistic nuclear collisions for investigating the initial conditions and transport characteristics of Quark-Gluon Plasma (QGP) [39–47]. This paper employs the AMPT model incorporating the string melting scenario. The model encompasses a sequence of processes, including the initial conditions of parton production, interactions among partons, hadronization through coalescence, and, finally, hadronic rescattering. More specifically, the nucleons are generated using the HIJING model [48] to establish their spatial and momentum distributions, after which they convert into partons. The interactions among these partons are governed by Zhang’s Parton Cascade model (ZPC) [49]. In this model, the parton-scattering cross-section σ can be characterized by the following:

$$\sigma = \frac{9\pi\alpha_s^2}{2\mu^2} \quad (5)$$

where α_s is the QCD coupling constant and μ is the screening mass. This cross-section delineates the dynamic expansion of the QGP phase. Subsequent to the parton cascade, partons combine to form hadrons, termed hadronization, employing a coalescence model [50]. Following hadronization, the interactions among the resulting hadrons in the final state are elucidated by the ART model [51].

The AMPT simulations for the Xe–Xe collisions are employed by parameterizing the nucleon density profile with Woods-Saxon distribution shown in Eq (4). To investigate the effect of nuclear deformation and diffuseness, and also the sensitivity to the system’s dynamic evolution, several sets of values for β_2 , γ , a_0 , and σ are used for comparisons. Here we use sets 1–4 to study the effect of nuclear deformations, i.e., by changing β_2 from 0 (spherical) to 0.18 (deformed, obtained from Ref. [30]) and changing γ from 0 (prolate) to 27° (triaxial) to 60° (oblate). Also, comparing the results from sets 2 ($a_0 = 0.57$ from Ref. [30]) and 5 ($a_0 = 0.492$ from Ref. [52]) can provide information for nuclear diffuseness. For the impact of transport properties, we use $\sigma = 3.0$ mb (set 6)[53, 54] instead of $\sigma = 6.0$ mb (set 3)[55]. The observables are shown in centrality dependence, where the centrality in this study is determined by the impact parameter in Xe–Xe collisions. More detailed information concerning the input parameters of the AMPT model can be found in table 1:

3 Analysis details

3.1 Observables

Experimentally, flow coefficients cannot be obtained directly via Eq. (2) but from two- and multi-particle correlations/cumulants[14, 56–58]:

$$v_n\{2\} \equiv \sqrt{c_n\{2\}} \quad (6)$$

Table 1. parameter sets used in this study

set	β_2	γ	a_0	σ
Set 1	0	0	0.57	6.0 mb
Set 2	0.18	0	0.57	6.0 mb
Set 3	0.18	27°	0.57	6.0 mb
Set 4	0.18	60°	0.57	6.0 mb
Set 5	0.18	0	0.492	6.0 mb
Set 6	0.18	27°	0.57	3.0 mb

where $c_n\{2\}$ is the two-particle cumulant. In this analysis, $v_2\{2\}, v_3\{2\}, v_4\{2\}$ are studied. In addition, the four-particle cumulants of v_n , denoted as $v_n\{4\}$, can be obtained via four-particle cumulants $c_n\{4\}$:

$$v_n\{4\} \equiv \sqrt[4]{-c_n\{4\}}. \quad (7)$$

The higher order cumulants of v_n are defined in a similar way, noted as $v_n\{6\}, v_n\{8\}$, etc. The two- and multi-particle cumulants of v_n have different contributions from flow fluctuations σ_{v_n} . It is well known that for the Gaussian type flow fluctuations and in the case $\sigma_{v_n} \ll \bar{v}_n$, we have [59]:

$$\begin{aligned} v_n\{2\}^2 &\approx \bar{v}_n^2 + \sigma_{v_n}^2, \\ v_n\{4\}^2 &\approx \bar{v}_n^2 - \sigma_{v_n}^2, \\ v_n\{6\}^2 &\approx \bar{v}_n^2 - \sigma_{v_n}^2, \\ v_n\{8\}^2 &\approx \bar{v}_n^2 - \sigma_{v_n}^2, \end{aligned} \quad (8)$$

here σ_{v_n} is the standard deviation of v_n distribution, which represents the event-by-event fluctuations of v_n . Then mean flow coefficient \bar{v}_n (which is also known as v_n from the flow symmetry plane) and the flow fluctuation σ_{v_n} can be extracted from the combination of $v_n\{2\}$ and $v_n\{4\}$ according to the Eq. (8):

$$\begin{aligned} \bar{v}_n &\approx \sqrt{\frac{v_n\{2\}^2 + v_n\{4\}^2}{2}}, \\ \sigma_{v_n} &\approx \sqrt{\frac{v_n\{2\}^2 - v_n\{4\}^2}{2}} \end{aligned} \quad (9)$$

For central and semi-central collisions, the lower order flow coefficients v_n (for $n = 2, 3$) are linearly correlated with the initial eccentricity coefficients ε_n [13, 60]. While higher harmonic flow v_n (for $n > 3$) not only has the linear response to the corresponding initial ε_n but also has contributions from the lower order ε_2 and/or ε_3 [61–63]. The latter is called the nonlinear flow mode. For example, V_4 and V_5 can be decomposed into the linear and nonlinear components:

$$\begin{aligned} V_4 &= V_4^{\text{NL}} + V_4^{\text{L}} \approx \chi_{4,22}(V_2)^2 + V_4^{\text{L}}, \\ V_5 &= V_5^{\text{NL}} + V_5^{\text{L}} \approx \chi_{5,32}V_2V_3 + V_5^{\text{L}}. \end{aligned} \quad (10)$$

Here V_n^{NL} and V_n^{L} are the nonlinear and linear (or called leftover) components, respectively. Their magnitudes are denoted as $v_{n,mk}$ and v_n^{L} . Besides, $\chi_{n,mk}$ is the nonlinear coefficient representing the strength of nonlinear response from lower order eccentricities [63]. The correlation between different order flow symmetry planes can

be studied by calculating the ratio between $v_{n,mk}$ and $v_n\{2\}$ [64]:

$$\begin{aligned}\rho_{4,22} &= \frac{v_{4,22}}{v_4\{2\}}, \\ \rho_{5,32} &= \frac{v_{5,32}}{v_5\{2\}}\end{aligned}\quad (11)$$

$\rho_{4,22}$ and $\rho_{5,32}$ can be used to study the correlations between Ψ_2 and Ψ_4 , as well as the correlations between three planes of Ψ_2 , Ψ_3 and Ψ_5 . The study of nonlinear flow modes, i.e., $v_{n,mk}$, $\rho_{n,mk}$, $\chi_{n,mk}$ have been performed before, they could provide further constraints on the initial conditions [14, 61, 65].

The correlations between v_n^2 and v_m^2 can be quantified via normalized symmetric cumulants NSC(m, n), defined as [14]:

$$\text{NSC}(m, n) = \frac{\langle v_m^2 v_n^2 \rangle - \langle v_m^2 \rangle \langle v_n^2 \rangle}{\langle v_m^2 \rangle \langle v_n^2 \rangle}, \quad (12)$$

where the angular bracket $\langle \rangle$ represents an average over all events. It allows to study if v_n^2 and v_m^2 are correlated, anti-correlated or uncorrelated, if $\text{NSC}(m, n) > 0$, < 0 and $= 0$, respectively. In this paper, NSC(3, 2) and NSC(4, 2) will be studied with the AMPT model to see if the results could bring extra information into the initial conditions and the structure of ^{129}Xe .

3.2 Multi-particle correlation

All the flow observables introduced in section 3.1 can be obtained via the multi-particle correlation method [14, 56–58]. To begin with, the flow coefficient v_n can be calculated using two-particle correlations:

$$v_n\{2\} \equiv \sqrt{c_n\{2\}} = \langle \langle \cos n(\varphi_1 - \varphi_2) \rangle \rangle^{1/2}, \quad (13)$$

where φ_1 and φ_2 are azimuthal angles from different particles. Double brackets $\langle \langle \rangle \rangle$ denote the average over all particles in an event and then the average over all events.

For multi-particle cumulants of v_n [58]:

$$\begin{aligned}v_n\{4\} &\equiv \sqrt[4]{-c_n\{4\}}, \\ v_n\{6\} &\equiv \sqrt[6]{\frac{1}{4}c_n\{6\}}, \\ v_n\{8\} &\equiv \sqrt[8]{-\frac{1}{33}c_n\{8\}}\end{aligned}\quad (14)$$

where :

$$\begin{aligned}c_n\{4\} &= \langle v_n^4 \rangle - 2\langle v_n^2 \rangle^2 \\ c_n\{6\} &= \langle v_n^6 \rangle - 9\langle v_n^4 \rangle \langle v_n^2 \rangle + 12\langle v_n^2 \rangle^3, \\ c_n\{8\} &= \langle v_n^8 \rangle - 16\langle v_n^6 \rangle \langle v_n^2 \rangle - 18\langle v_n^4 \rangle^2 + 144\langle v_n^4 \rangle \langle v_n^2 \rangle^2 - 144\langle v_n^2 \rangle^4\end{aligned}\quad (15)$$

and

$$\begin{aligned}\langle v_n^4 \rangle &= \langle \langle \cos(n\varphi_1 + n\varphi_3 - n\varphi_2 - n\varphi_4) \rangle \rangle, \\ \langle v_n^6 \rangle &= \langle \langle \cos(n\varphi_1 + n\varphi_3 + n\varphi_5 - n\varphi_2 - n\varphi_4 - n\varphi_6) \rangle \rangle, \\ \langle v_n^8 \rangle &= \langle \langle \cos(n\varphi_1 + n\varphi_3 + n\varphi_5 + n\varphi_7 - n\varphi_2 - n\varphi_4 - n\varphi_6 - n\varphi_8) \rangle \rangle\end{aligned}\quad (16)$$

The magnitude of nonlinear flow mode $v_{n,mk}$ could be obtained via the multi-particle correlations [63, 64]. For $n = 4, 5$, which is studied in this paper, we have:

$$\begin{aligned} v_{4,22} &= \frac{\langle\langle\cos(4\varphi_1 - 2\varphi_2 - 2\varphi_3)\rangle\rangle}{\sqrt{\langle\langle\cos(2\varphi_1 + 2\varphi_2 - 2\varphi_3 - 2\varphi_4)\rangle\rangle}}, \\ v_{5,32} &= \frac{\langle\langle\cos(5\varphi_1 - 3\varphi_2 - 2\varphi_3)\rangle\rangle}{\sqrt{\langle\langle\cos(3\varphi_1 + 2\varphi_2 - 3\varphi_3 - 2\varphi_4)\rangle\rangle}} \end{aligned} \quad (17)$$

They quantify the magnitude of the nonlinear mode in high-order flow coefficients. By subtracting $v_{4,22}$ and $v_{5,32}$ from v_4 , and v_5 , respectively, we can easily calculate the magnitude of linear modes:

$$\begin{aligned} v_4^L &= \sqrt{v_4^2\{2\} - v_{4,22}^2}, \\ v_5^L &= \sqrt{v_5^2\{2\} - v_{5,32}^2} \end{aligned} \quad (18)$$

Nonlinear coefficient $\chi_{n,mk}$ also describes the nonlinear contributions but is independent of v_2 and v_3 . It can be derived by taking the ratio of $v_{n,mk}$ and corresponding lower-order v_n ($n = 2, 3$):

$$\begin{aligned} \chi_{4,22} &= \frac{v_{4,22}}{\sqrt{\langle v_2^4 \rangle}} = \frac{\langle\langle\cos(4\varphi_1 - 2\varphi_2 - 2\varphi_3)\rangle\rangle}{\langle\langle\cos(2\varphi_1 + 2\varphi_2 - 2\varphi_3 - 2\varphi_4)\rangle\rangle}, \\ \chi_{5,32} &= \frac{v_{5,32}}{\sqrt{\langle v_2^2 v_3^2 \rangle}} = \frac{\langle\langle\cos(5\varphi_1 - 3\varphi_2 - 2\varphi_3)\rangle\rangle}{\langle\langle\cos(3\varphi_1 + 2\varphi_2 - 3\varphi_3 - 2\varphi_4)\rangle\rangle} \end{aligned} \quad (19)$$

The $\rho_{n,mk}$, correlation between different order flow symmetry planes can be obtained by taking Eqs. (13) and (17):

$$\begin{aligned} \rho_{4,22} &= \frac{v_{4,22}}{v_4\{2\}} = \frac{\langle\langle\cos(4\varphi_1 - 2\varphi_2 - 2\varphi_3)\rangle\rangle}{\sqrt{\langle\langle\cos(2\varphi_1 + 2\varphi_2 - 2\varphi_3 - 2\varphi_4)\rangle\rangle}\langle\langle\cos(4\varphi_1 - 4\varphi_2)\rangle\rangle}, \\ \rho_{5,32} &= \frac{v_{5,32}}{v_5\{2\}} = \frac{\langle\langle\cos(5\varphi_1 - 3\varphi_2 - 2\varphi_3)\rangle\rangle}{\sqrt{\langle\langle\cos(3\varphi_1 + 2\varphi_2 - 3\varphi_3 - 2\varphi_4)\rangle\rangle}\langle\langle\cos(5\varphi_1 - 5\varphi_2)\rangle\rangle} \end{aligned} \quad (20)$$

Expanding Eq. (12) with multi-particle correlations, normalized symmetric cumulants $\text{NSC}(m, n)$ can be expressed as:

$$\text{NSC}(m, n) = \frac{\langle\langle\cos(m\varphi_1 + n\varphi_3 - m\varphi_2 - n\varphi_4)\rangle\rangle - \langle\langle\cos(m\varphi_1 - m\varphi_3)\rangle\rangle\langle\langle\cos(n\varphi_2 - n\varphi_4)\rangle\rangle}{\langle\langle\cos(m\varphi_1 - m\varphi_3)\rangle\rangle\langle\langle\cos(n\varphi_2 - n\varphi_4)\rangle\rangle}$$

All these observables are now expressed in terms of 2- and multi-particle correlations and then can be calculated using the *Generic Framework* [14, 66] or its latest implementation *Generic Algorithm* [58].

4 Results

4.1 Study on the nuclear deformation

The centrality dependence of $v_2\{2\}$ and $v_3\{2\}$ in Xe-Xe collisions at 5.44 TeV are shown in Fig. 1. Here, $v_2\{2\}$ increases significantly in the Ultra-Central Collisions (UCC) region when changing β_2 from 0 (red diamonds) to 0.18 (the other markers). In

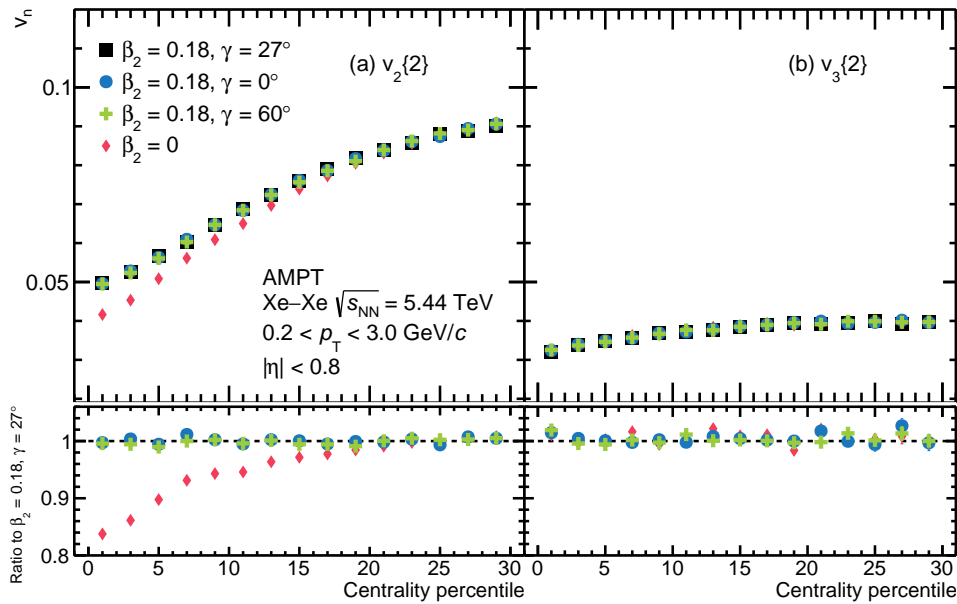


Fig. 1. Centrality dependence of $v_n\{2\}$ ($n = 2, 3$) in Xe–Xe collisions at $\sqrt{s_{\text{NN}}} = 5.44$ TeV in AMPT.

the UCC region, where the two colliding nuclei almost fully overlap, the eccentricity of the overlapping region is determined by the shape or nuclear structure of the colliding nuclei. As it's well known, the β_2 parameter in the Woods-Saxon distribution characterizes an elliptical shape of the Woods-Saxon nucleon density profile. A non-zero β_2 of ^{129}Xe enhances the initial eccentricity ε_2 compared to the one with a spherical shape where $\beta_2 = 0$ and consequently leads to an increase in v_2 because of the linear correlation between ε_n and v_n , i.e., $v_n \propto \varepsilon_n$, for $n = 2$ or 3 [67, 68]. In Fig. 1(b), $v_3\{2\}$ has negligible differences when changing the β_2 values, because the triangularity ε_3 of the overlapping region does not depend on β_2 [24].

Figure 1 also shows consistent results of $v_n\{2\}$ ($n = 2, 3$) with variations in the tri-axial parameter γ across the 0–30% centrality range. This is not a surprise, as probing the 3-D structure usually requests correlation involving more than two particles. In light of preceding investigations [22], a potential sensitivity of ε_2 to γ was indicated for centrality range 0–0.2%, as concluded from simulations using the initial-state model. However, the current study refrains from probing such phenomena, relying on the AMPT model's final state information. The intrinsic computational demands inherent to capturing the entirety of the dynamic evolution process within AMPT serve as a significant impediment.

The value of $v_2\{2\}$ receives the contributions not only from the initial eccentricity ε_2 but also from the event-by-event eccentricity fluctuations. To undertake a more comprehensive exploration of the ramifications imposed by the initial event-by-event eccentricity fluctuations and correspondingly the final state elliptic flow fluctuations, the utilization of both $v_2\{2\}$ and $v_2\{4\}$ is employed. This combined approach is particularly insightful as these two observables carry opposite contributions from flow fluctuations, as shown in Eqs. (8). As a result, the centrality dependence of $v_2\{4\}$, as well as the \bar{v}_2 and σ_{v_2} in Xe–Xe collisions at 5.44 TeV are presented in Fig. 2. As shown in Fig. 2(a), $v_2\{4\}$ exhibits a slight increase when changing β_2 from 0 (red

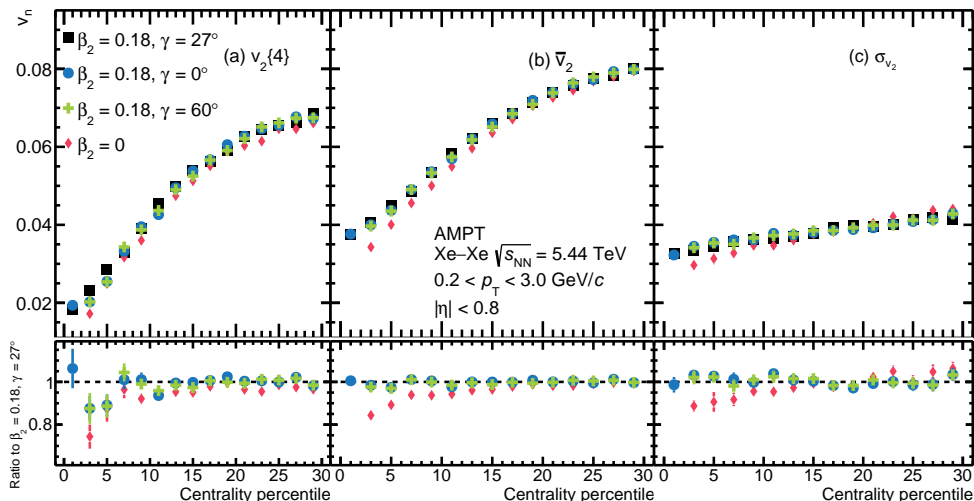


Fig. 2. Centrality dependence of $v_2\{4\}$, \bar{v}_2 , σ_{v_2} in Xe–Xe collisions at $\sqrt{s_{NN}} = 5.44$ TeV in AMPT.

diamonds) to 0.18 (the other markers), despite the sizable statistical uncertainties in the presented centrality region. It was previously suggested that $v_2\{4\}$ is influenced by the nuclear diffuseness a_0 , with a weak sensitivity to β_2 using different nuclei at the RHIC energy [25]. This aligns with our AMPT results shown in Figs. 2(a) and 9(a). In Fig. 2(b)(c), \bar{v}_2 and σ_{v_2} have significant increases in UCC region when changing β_2 from 0 to 0.18. The sensitivity of \bar{v}_2 to β_2 primarily arises from its linear correlation with ε_2 . In the case of flow fluctuations σ_{v_2} , a deformed nucleus assumes varied orientations compared to a spherical shape. These random orientations result in stronger fluctuations of the elliptic flow.

In Fig. 2, $v_2\{4\}$, \bar{v}_2 , and σ_{v_2} stay unchanged with variations in γ . These observables do not lend themselves to the task of constraining the unique triaxial parameter characterizing the nucleus ^{129}Xe .

An evident sensitivity of $v_2\{6\}$ to β_3 is reported in a previous study [25]. The same work also discusses the correlation between the sensitivity of β_n and the number of particles used in the multi-particle correlations. Following the same concept, it is expected that observables like $v_2\{6\}$ and $v_2\{8\}$ may yield distinctive insights into the nuclear structure, compared to $v_2\{2\}$ and $v_2\{4\}$ discussed above. The centrality dependence of $v_2\{6\}$ and $v_2\{8\}$ are shown in Fig. 3. Amidst the sizable uncertainties, the current study refrains from drawing a firm conclusion regarding the sensitivity of these two observables to either β_2 or γ across the 0–30% centrality interval.

The v_n with multi-particle correlations, i.e., $v_2\{4\}$, $v_2\{6\}$, and $v_2\{8\}$, were reported to exhibit a slight difference at the precision of 1-2% in Pb–Pb collisions [69]. This difference is believed to have originated from the deviations from a Bessel-Gaussian shape, particularly a non-zero skewness of the event-by-event v_2 distribution. To determine whether a similar pattern persists in Xe–Xe collisions and explore the discrepancies between higher-order multi-particle cumulants, the ratios $v_2\{m\}/v_2\{4\}$ for $m = 2, 6$, and 8 are presented as a function of centrality in Fig. 4. The ratio of $v_2\{2\}/v_2\{4\}$ increases dramatically toward the central region in Fig. 4(a). Such an increase is dominated by flow fluctuations in the most central region. Although the sensitivity of $v_2\{2\}/v_2\{4\}$ to β_2 and γ is covered by uncertainties, a weak sensitivity to β_2 was observed previously in a similar study in U–U collisions at $\sqrt{s_{NN}} =$

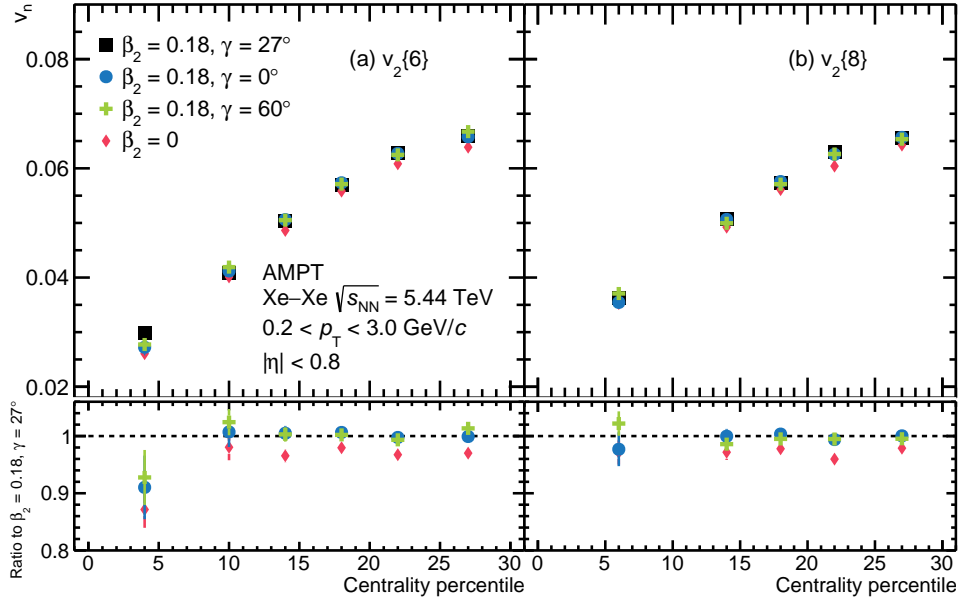


Fig. 3. Centrality dependence of $v_2\{6\}$, $v_2\{8\}$ in Xe–Xe collisions at $\sqrt{s_{\text{NN}}} = 5.44$ TeV in AMPT.

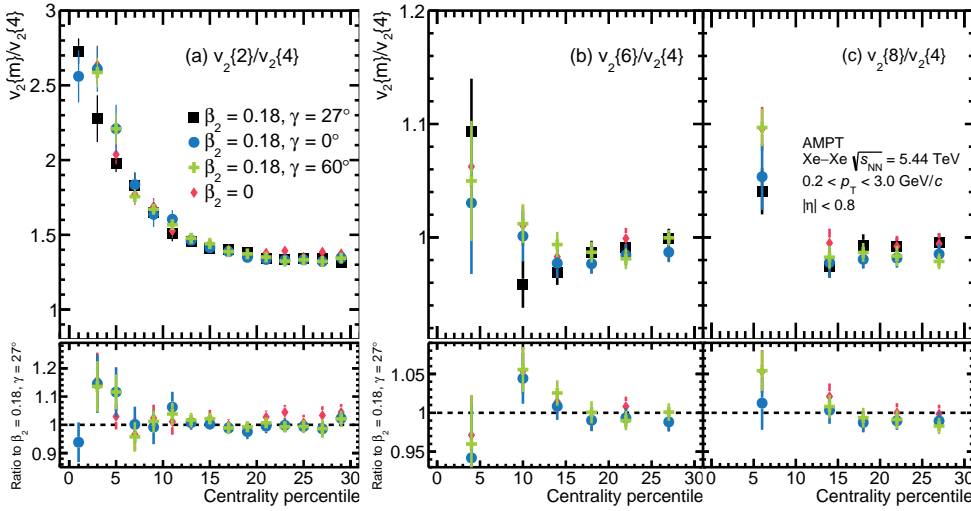


Fig. 4. Centrality dependence of $v_2\{2\}/v_2\{4\}$ in Xe–Xe collisions at $\sqrt{s_{\text{NN}}} = 5.44$ TeV in AMPT.

193 GeV [26]. Subsequent investigations with increased statistics are anticipated to elucidate the presence of this sensitivity. However, the current study is constrained by the substantial computing demands involved. Concerning higher-order cumulants with $m=6,8$, the ratios $v_2\{6\}/v_2\{4\}$ and $v_2\{8\}/v_2\{4\}$ are close to unity within uncertainties and they stay unchanged when varying the nuclear structure configurations β_2 and γ .

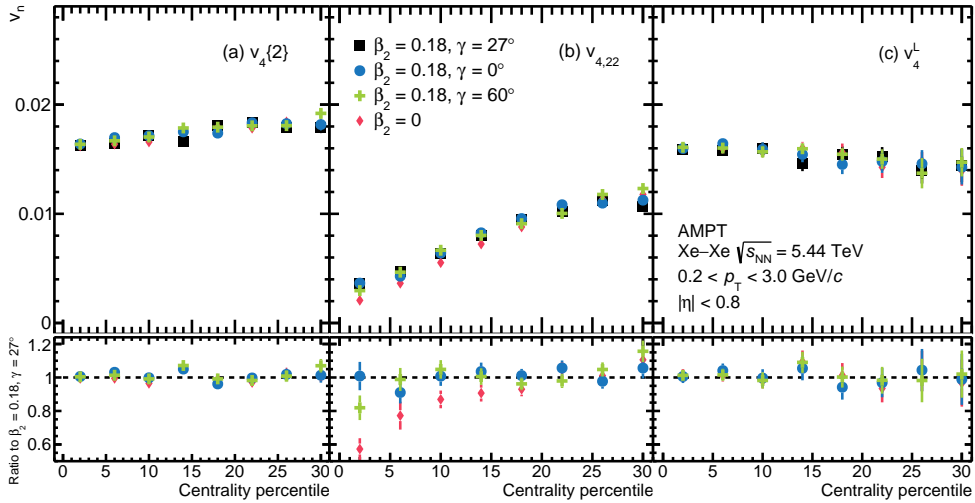


Fig. 5. Centrality dependence of nonlinear modes including (a) v_4 , (b) $v_{4,22}$ and (c) Linear v_4 in Xe–Xe collisions at $\sqrt{s_{\text{NN}}} = 5.44$ TeV in AMPT.

In the context of the higher harmonic flow ($n > 3$), such as v_4 , it consists of a linear constituent v_4^{L} stemming from the initial ε_4 and a nonlinear component v_4^{NL} originating from ε_2^2 . The centrality dependence of $v_4\{2\}$, v_4^{L} , and v_4^{NL} or denoted as $v_{4,22}$ are presented in Figure 5. In Fig. 5(a)(b), $v_4\{2\}$ and $v_{4,22}$ exhibit an increasing trend moving from the central to the mid-central collision, while v_4^{L} in Fig. 5(c) has a flat distribution in the presented centrality region. Notably, a comparison of the magnitudes of $v_4\{2\}$ and v_4^{L} reveals the prevailing dominance of v_4^{L} over $v_{4,22}$ in central collisions, while in the mid-central region $v_{4,22}$ converges with v_4^{L} . This is consistent with previous measurements in Pb–Pb collisions at the LHC [64]. The linear component v_4^{L} shows an absence of sensitivity to the quadrupole deformation parameter β_2 across the 0–30% centrality range. A similar observation has been reported recently in Ref. [26], where both v_4^{L} and $v_4\{2\}$ show no sensitivity to β_2 . In contrast, the sensitivity of both $v_{4,22}$ and v_4^{L} to the hexadecapole deformation parameter β_4 is seen [26], owing to their shared provenance from ε_4 . The nonlinear component $v_{4,22}$, as illustrated in Fig. 5(b), manifests a degree of 20% reductions with zero β_2 within the UCC region, albeit with a magnitude smaller than that of $v_4\{2\}$. Since the nonlinear flow $v_{n,mk}$ probes a smaller spatial distribution than the flow coefficient v_n , it can impose more stringent constraints on initial conditions and nuclear structure parameters. Variations in γ parameter show that $v_{4,22}$, v_4^{L} , and the $v_4\{2\}$ all exhibit diminished sensitivities to γ within the 0–30% centrality range, and thus they are unable to probe the triaxial nuclear structure.

The nonlinear coefficient $\chi_{4,22}$, defined in Eq. (10), is not solely affected by transport properties but also by initial conditions [70]. It previously exhibits a weak dependence on nuclear deformation β_2 in central collisions at the RHIC isobar runs [26, 27, 71]. Verifying whether the same conclusion holds in the context of Xe–Xe collisions remains pertinent. Nonlinear correlation $\rho_{4,22}$, introduced in Eq. (11), demonstrates an insensitivity to the influences of final state interactions [70], rendering it an effective tool for probing initial conditions. In Fig. 6, the centrality dependence of $\chi_{4,22}$ and $\rho_{4,22}$ are presented. In panel (a), $\chi_{4,22}$ stays unchanged with different nuclear structure configurations in the presented centrality region despite the large uncertainties in the central collisions. Considering the relationship $V_4^{\text{NL}} = \chi_{4,22} (V_2)^2$, the

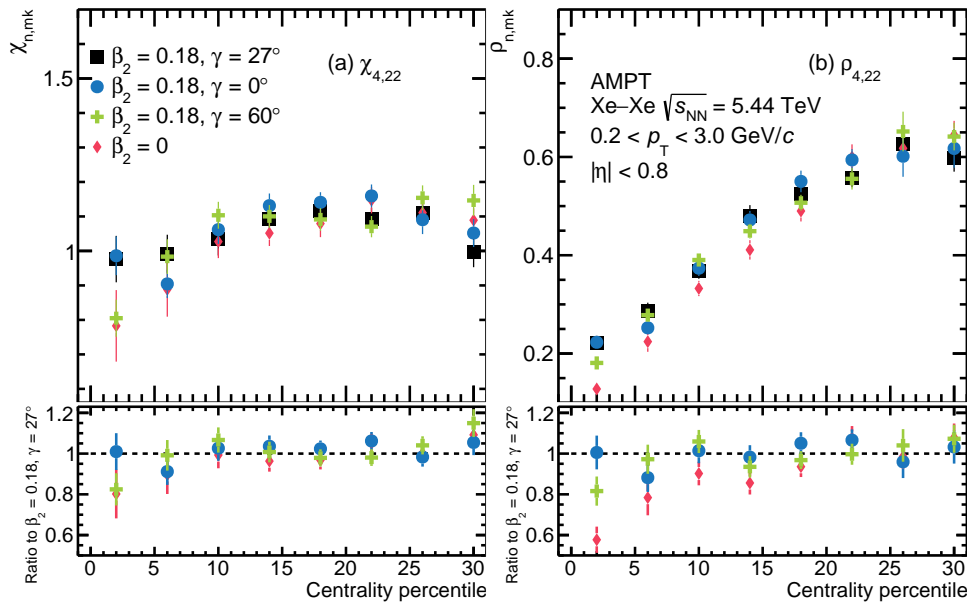


Fig. 6. Centrality dependence of nonlinear modes including (a) $\chi_{4,22}$ and (b) $\rho_{4,22}$ in Xe–Xe collisions at $\sqrt{s_{\text{NN}}} = 5.44$ TeV in AMPT.

sensitivity of $v_{4,22}$ to β_2 primarily stems from the sensitivity conveyed by $(V_2)^2$. A similar scenario can be observed in the case of $v_{5,32}$ and $\chi_{5,32}$, as shown in Fig.15 in the appendix, suggesting that the sensitivity arises from v_2v_3 . Furthermore, the results in Fig. 1 have already indicated that v_3 is insensitive to β_2 , thereby emphasizing that the dominant sensitivity of $v_{5,32}$ to β_2 emerges from v_2 . In Fig. 6(b), $\rho_{4,22}$ shows a distinct drop with $\beta_2=0$ in UCC region. This reduction is caused by the $v_{4,22}$ in Fig. 5(b) with $\beta_2=0$, as $\rho_{4,22} = v_{4,22}/v_4\{2\}$ and no such sensitivity is observed in $v_4\{2\}$. Turning to a physics view, $\rho_{4,22}$ signifies the correlation between Ψ_4 and Ψ_2 . When the initial geometry is spherical ($\beta_2 = 0$), Ψ_4 and Ψ_2 could be arbitrary orientations and thus have negligible correlations. When the geometry has an anisotropy ($\beta_2 > 0$), they will have specific orientations. As a result, their correlation increases as well. Changing triaxial parameter γ , the results of $\chi_{4,22}$ and $\rho_{4,22}$ remain consistent within errors, restraining themselves from an ideal probe of the triaxial structure of ^{129}Xe .

Normalized symmetric cumulant (NSC) quantifies the correlation between different order flow coefficients and has been systematically studied in Pb–Pb collisions [72–74]. It was found that NSC(3, 2) is insensitive to the dynamic evolution but carries unique sensitivity to initial conditions [72, 73]. Thus, it is potentially a good probe of the nuclear structure. In fact, NSC(3, 2) has been previously studied in the U–U collisions, showing its sensitivity to β_2 [26]. While for NSC(4, 2), it is sensitive to both initial conditions and transport properties [72, 73]. In Figure 7(a), a tiny (and insignificant) increase can be observed in NSC(3, 2) by decreasing the β_2 value from 0.18 to 0, and no significant variation is observed when changing γ . This indicates that the anti-correlation between $\langle v_3^2 \rangle$ and $\langle v_2^2 \rangle$ is reduced by quadrupole deformation and is independent of γ . For Fig. 7(b), it is evident that NSC(4, 2) exhibits little to no sensitivity to either β_2 or γ , suggests that the correlation between $\langle v_4 \rangle$ and $\langle v_2 \rangle$ remains relatively independent of nuclear deformation.

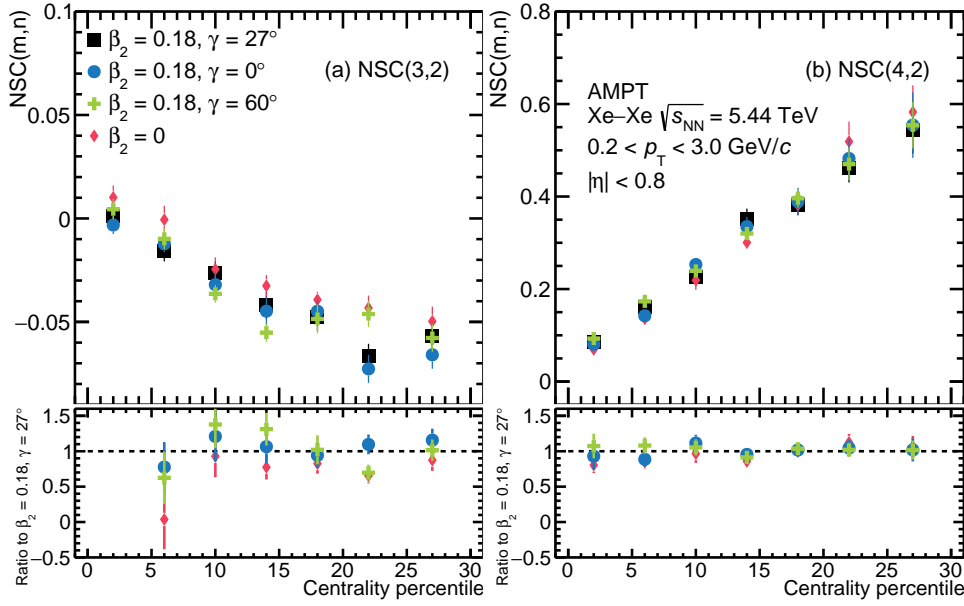


Fig. 7. Centrality dependence of $NSC(m, n)$ in Xe–Xe collisions at $\sqrt{s_{NN}} = 5.44$ TeV in AMPT.

4.2 Study on the nuclear diffuseness

The radial profile of the nucleus is determined by either the nuclear diffuseness a_0 or the radius R_0 , both of which impact the initial spatial anisotropy and consequently influence the flow observables. Recent studies have highlighted the significant impact of a_0 on various flow observables in the mid-central region (20–60% centrality)[25], underscoring the importance of verifying this within the context of Xe–Xe collisions using the AMPT model. This section delves into the potential of flow observables in investigating the a_0 introduced in Eq. (4). Generally, a larger nuclear diffuseness a_0 results in a significantly increased total hadronic cross-section, leading to a more diffused QGP.

Fig. 8 shows the centrality dependence of $v_2\{2\}$ and $v_3\{2\}$ in Xe–Xe collisions at 5.44 TeV using two distinct values of a_0 . Calculations with larger a_0 values (presented by black markers) lead to smaller v_2 results in the semi-central collisions, which is agreed with the results in the isobar runs of Ru–Ru/Zr–Zr [25]. Meanwhile, no obvious change in v_3 is seen after changing the a_0 values across the 0–60% centrality range.

As discussed in section 4.1, the increase of σ_{v_2} is mainly due to the random orientations of deformed nuclei and is expected to be less influenced by the diffuseness of nuclei. To verify this, the results of $v_2\{4\}$, \bar{v}_2 , and σ_{v_2} are presented in Fig. 9. It is observed that $v_2\{4\}$ and \bar{v}_2 are reduced by larger a_0 in the semi-central region, while σ_{v_2} remains the same. This observation aligns with our earlier discussion, affirming that the diffuseness primarily impacts the eccentricity rather than its fluctuations.

In exploring a_0 , we can split v_4 into its linear and nonlinear components to see how they respond differently to changes in a_0 . Figure 10 shows the centrality dependence of $v_4\{2\}$ and its linear and nonlinear components. A larger a_0 value reduces both $v_4\{2\}$ and $v_{4,22}$ in 20–40% centrality. Figure 10(c) does not show the sensitivity of v_4^L to a_0 due to the large uncertainties. The reduction of the nonlinear part $v_{4,22}$ affects $v_4\{2\}$. This is different from what we saw for β_2 . Also, it is seen that $v_{4,22}$ is much

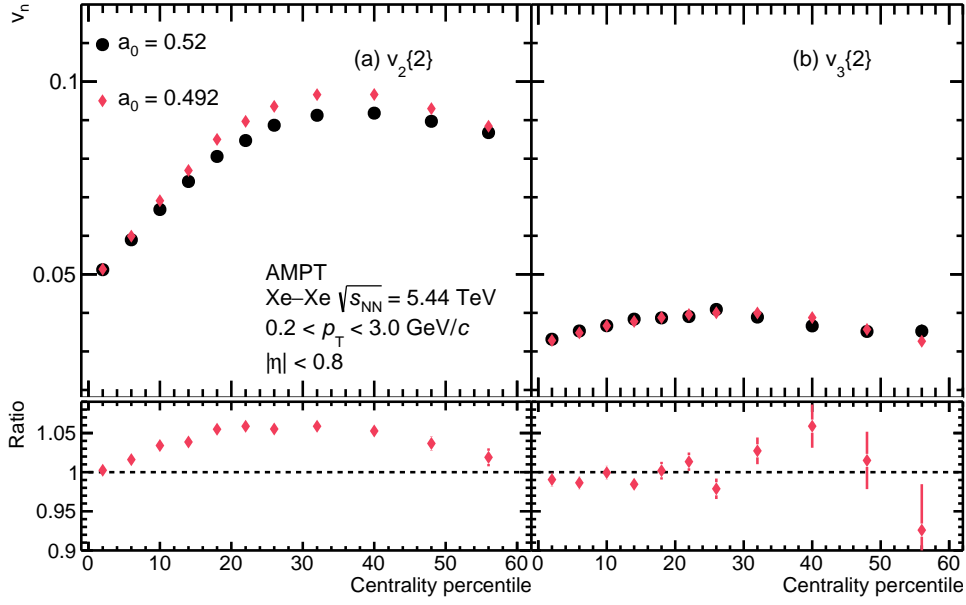


Fig. 8. Centrality dependence of $v_n\{2\}$ ($n = 2, 3$) in Xe–Xe collisions at $\sqrt{s_{NN}} = 5.44$ TeV in AMPT.

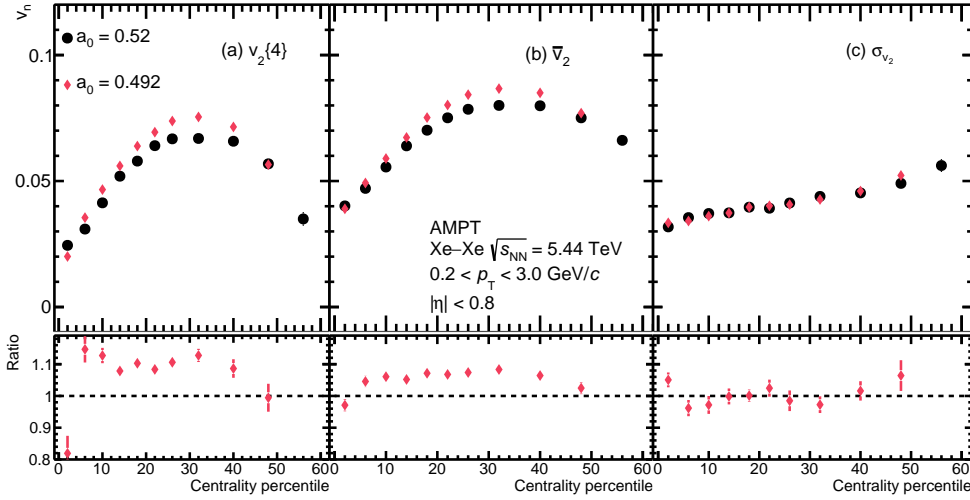


Fig. 9. Centrality dependence of $v_2\{4\}$, \bar{v}_2 , σ_{v_2} in Xe–Xe collisions at $\sqrt{s_{NN}} = 5.44$ TeV in AMPT.

smaller than v_4^L in the most central region, so we do not see any effect of β_2 on $v_4\{2\}$ even though β_2 increases $v_{4,22}$ significantly in that region. For a_0 , more sensitivity is found in the mid-central collisions, where the nonlinear component $v_{4,22}$ is about half of the total $v_4\{2\}$, and how it changes with a_0 has a bigger effect on $v_4\{2\}$ in this region.

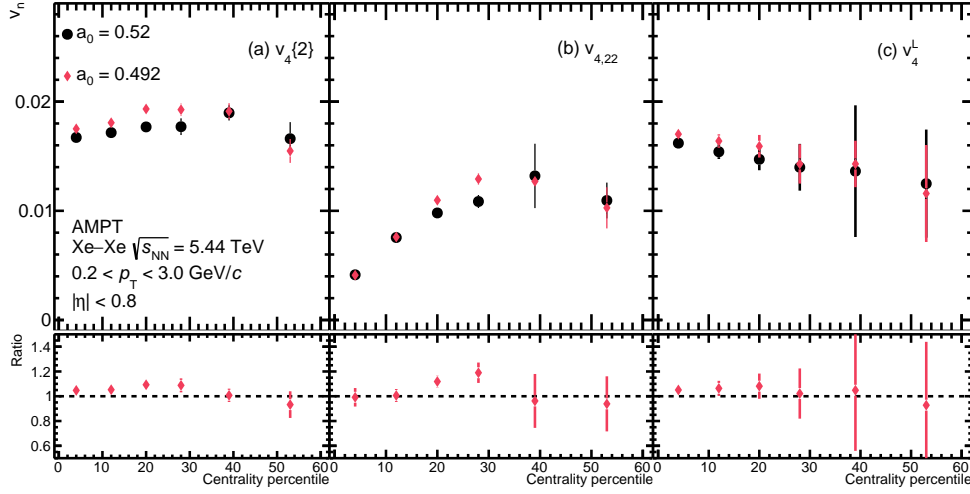


Fig. 10. Centrality dependence of nonlinear modes including (a) v_4 , (b) $v_{4,22}$ and (c) Linear v_4 in Xe-Xe collisions at $\sqrt{s_{NN}} = 5.44$ TeV in AMPT.

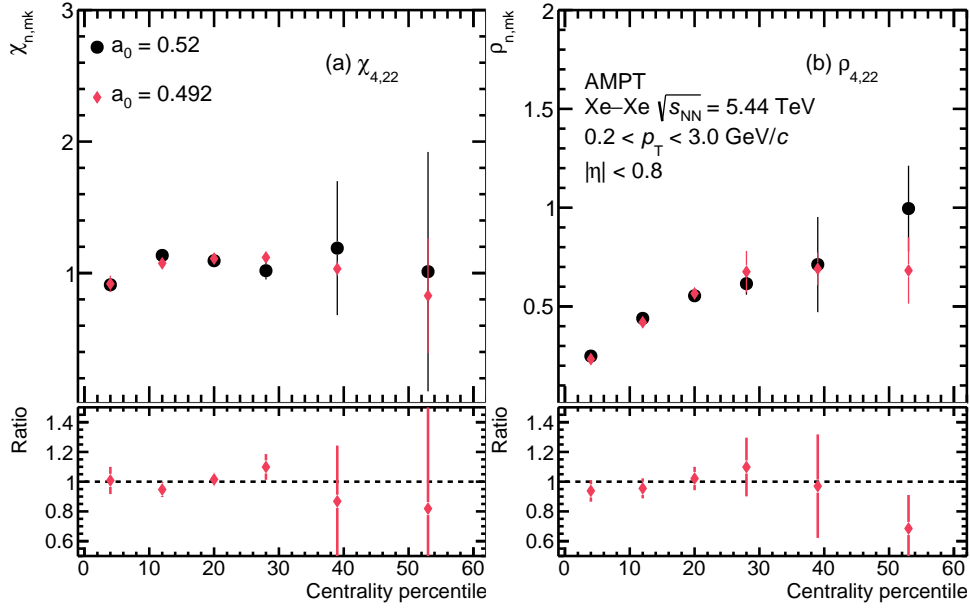


Fig. 11. Centrality dependence of nonlinear modes including (a) $\chi_{4,22}$ and (b) $\rho_{4,22}$ in Xe-Xe collisions at $\sqrt{s_{NN}} = 5.44$ TeV in AMPT.

As also introduced in section 4.1, $\chi_{4,22}$ is not only affected by dynamic evolution but also by initial conditions, while $\rho_{4,22}$ only depends on the initial state. It is crucial to check if the nonlinear modes can probe the initial conditions, particularly the diffuseness of nuclei. Here $\chi_{4,22}$ and $\rho_{4,22}$ with different a_0 are presented in Fig. 11. Neither of them is affected by a_0 in 0–60% centrality region. As $\rho_{4,22} = v_{4,22}/v_4\{2\}$, the sensitivity to a_0 is, to a large extent, canceled by taking this ratio. The insensitivity

of $\chi_{4,22}$ to a_0 can lead to similar conclusion as in the discussion of β_2 that the sensitivity of $v_{4,22}$ to a_0 is mainly due to the V_2^2 term in $V_4^{\text{NL}} \approx \chi_{4,22}(V_2)^2$.

Because of the limited statistics, there are large uncertainties in the results of NSC(3,2) and NSC(4,2), and no firm conclusion about how sensitive they are to the a_0 parameter can be drawn. Thus, the results are not presented and discussed here but added in the appendix.

4.3 Influence from the transport properties

The results shown in this study have indicated that $v_2\{2\}$, \bar{v}_2 , σ_{v_2} , $v_{4,22}$ and $\rho_{4,22}$ can potentially probe the nuclear deformation, meanwhile $v_2\{2\}$, $v_2\{4\}$, \bar{v}_2 , $v_4\{2\}$, $v_{4,22}$ have the ability to study nuclear diffuseness a_0 . In order to achieve unbiased constraints on the nuclear structure parameters in experiments, one must ensure that the chosen observables are only sensitive to the initial conditions and not influenced by the dynamic evolution of the created system. In particular, it has been found in the study at RHIC isobar runs that the ratio observables in Zr–Zr and Ru–Ru can largely cancel out the effects of final state interactions and thus reflect mainly the impact from the initial stages. Here we present the mentioned observables ($v_2\{2\}$, $v_2\{4\}$, \bar{v}_2 , σ_{v_2} , $v_4\{2\}$, $v_{4,22}$, $\rho_{4,22}$) in the ratio of Xe–Xe/Pb–Pb, checking if the ratio of two collision system minimizes the influence of dynamic evolution.

In Fig. 12, the centrality dependence of $v_2\{2\}$, $v_2\{4\}$, \bar{v}_2 and σ_{v_2} in the ratio of Xe–Xe/Pb–Pb collisions are presented, using two different partonic cross sections. The bottom panels of each figure show the ratio of the results using 3 mb and 6 mb (“double ratio”). The ratios in Fig. 12 are all consistent with unity, indicating that these observables, including $v_2\{2\}$, $v_2\{4\}$, \bar{v}_2 , σ_{v_2} , in the ratio of Xe–Xe/Pb–Pb are less dependent on the dynamic evolution and potentially are good probes to initial conditions.

In addition, $v_4\{2\}$ and its nonlinear modes $v_{4,22}$ and $\rho_{4,22}$ in the ratio of Xe–Xe/Pb–Pb are also investigated, the centrality dependence is presented in Fig. 13. Despite large uncertainties, the results with different partonic cross sections are consistent with each other, and the “double ratio” is compatible with unity. Such results show that $v_4\{2\}$, $v_{4,22}$, $\rho_{4,22}$ in the ratio of Xe–Xe/Pb–Pb might be not affected by dynamic evolution. Considering $v_4\{2\}$ and $v_{4,22}$ are sensitive to a_0 in the mid-central region, while $v_{4,22}$ and $\rho_{4,22}$ are enhanced by non-zero β_2 in the most central region, these observables are valuable in the exploration of initial conditions and nuclear structure parameters.

5 Summary

This paper presents a comprehensive exploration of the influence of nuclear deformation and nuclear diffuseness on various flow observables in Xe–Xe collisions at $\sqrt{s_{\text{NN}}} = 5.44$ TeV, using AMPT event generator. We observe that the elliptic flow coefficients $v_2\{2\}$, \bar{v}_2 , elliptic flow fluctuation σ_{v_2} , as well as the nonlinear flow mode observables $v_{4,22}$ and $\rho_{4,22}$, are enhanced in central collisions in the presence of nuclear quadrupole deformation β_2 . These enhancements come from the increased eccentricities and their fluctuations in the initial geometry in the presence of a deformed shape of ^{129}Xe . Thus, the aforementioned flow observables can potentially constrain nuclear deformation through data-model comparisons in high-energy heavy-ion collisions in the near future. On the other hand, most flow observables do not exhibit much sensitivity to the triaxiality parameter, underscoring the importance of utilizing combined flow observables like $v_n - [p_{\text{T}}]$ correlations in future studies.

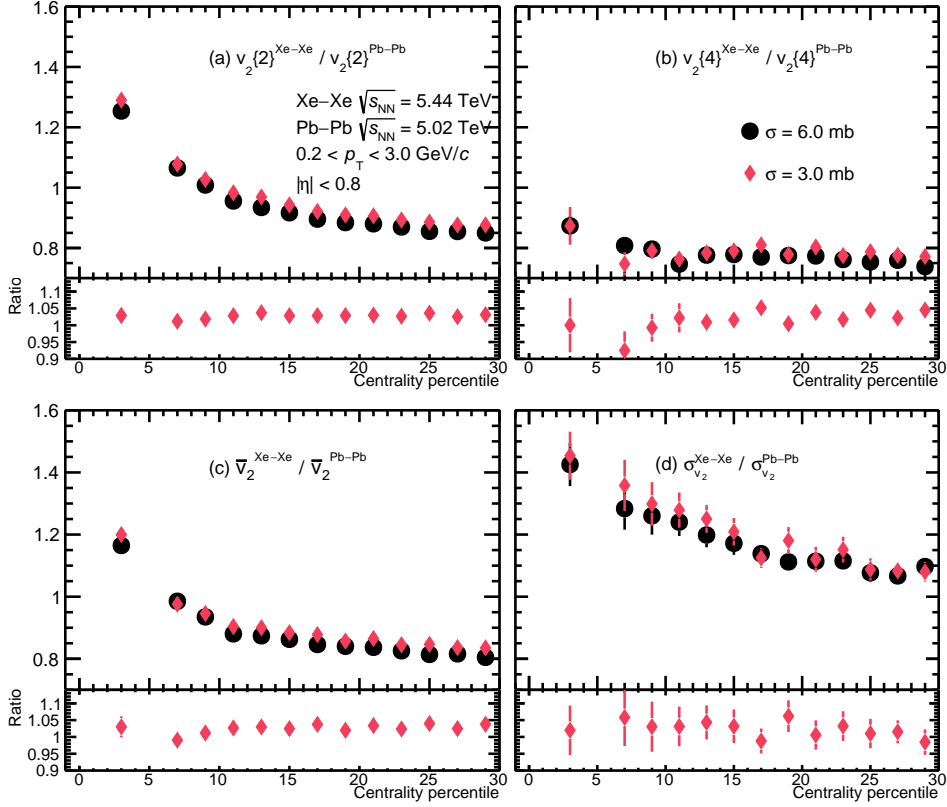


Fig. 12. Centrality dependence of $v_2\{2\}$, $v_2\{4\}$, \bar{v}_2 , σ_{v_2} in Xe–Xe, Pb–Pb collisions at $\sqrt{s_{\text{NN}}} = 5.44$ TeV and $\sqrt{s_{\text{NN}}} = 5.02$ TeV respectively in AMPT. The lower panels also present the ratio of different partonic cross sections.

In addition, larger nuclear diffuseness a_0 for ^{129}Xe leads to smaller values in $v_2\{2\}$, \bar{v}_2 , $v_4\{2\}$, $v_{4,22}$, and v_2 with multi-particle correlations ($v_2\{4\}$, $v_2\{6\}$, $v_2\{8\}$) in mid-central collisions. Among them, $v_4\{2\}$, $v_2\{4\}$, $v_2\{6\}$, and $v_2\{8\}$ are only sensitive to a_0 , while σ_{v_2} and $\rho_{4,22}$ are only sensitive to β_2 . The differing sensitivities of these observables allow for separating constraints on the values of a_0 and β_2 , which will help fine-tune other model parameters and enable more precise predictions.

We also investigate the influence of dynamic evolution on flow observables by varying the parton cross-section in the AMPT model. The parton cross-section does not significantly affect most of the observables in the ratio of Xe–Xe/Pb–Pb, indicating that the final state effect is canceled out when comparing the two collision systems. Future collisions of different nuclear species at varying energies will provide more insights into heavy ion collisions and improve our nuclear structure knowledge.

6 Acknowledgements

M. Zhao and Y. Zhou are funded by the European Union (ERC, InitialConditions), VILLUM FONDEN (grant number 00025462), and Danmarks Frie Forskningsfond (Independent Research Fund Denmark). J. Jia’s work is supported by the US Department of Energy (grant number DE-FG02-87ER40331).

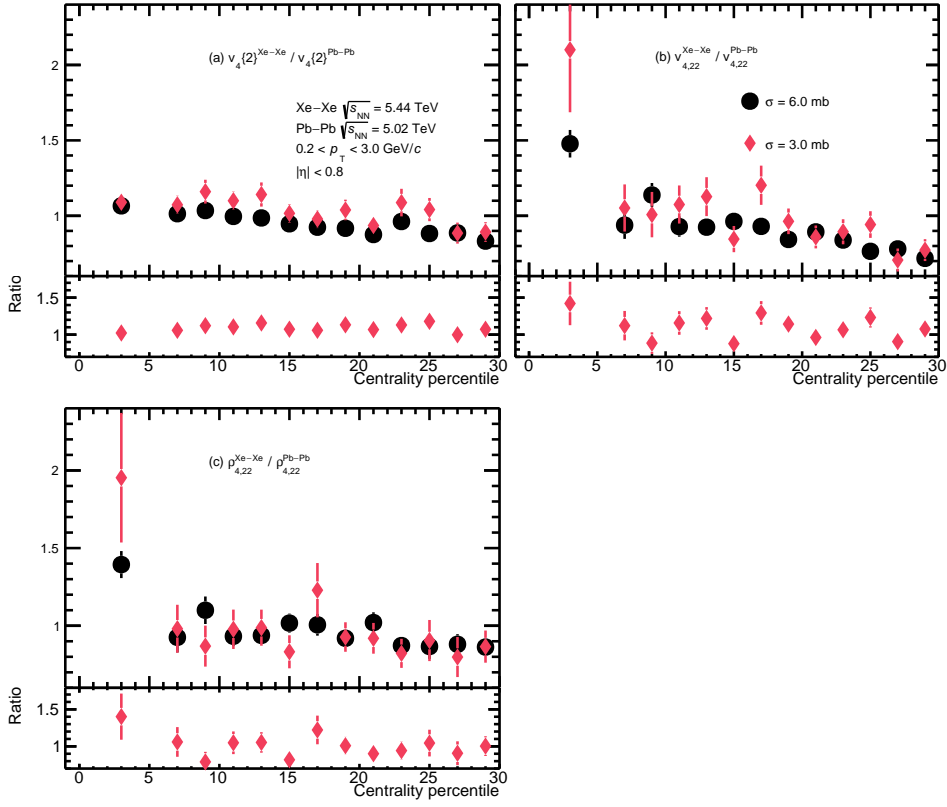


Fig. 13. Centrality dependence of $v_4\{2\}$, $v_{4,22}$, $\rho_{4,22}$ in Xe-Xe, Pb-Pb collisions at $\sqrt{s_{\text{NN}}} = 5.44$ TeV and $\sqrt{s_{\text{NN}}} = 5.02$ TeV respectively in AMPT. The ratio of different partonic cross sections is also presented in the lower panels.

7 Appendix

7.1 nuclear deformation

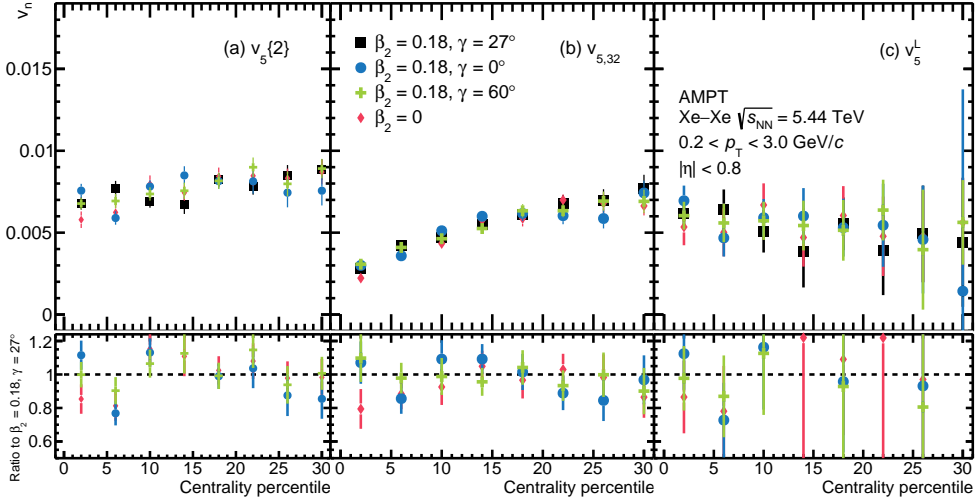


Fig. 14. Centrality dependence of nonlinear modes including (a) v_5 , (b) $v_{5,32}$ and (c) Linear v_5 in Xe–Xe collisions at $\sqrt{s_{\text{NN}}} = 5.44$ TeV in AMPT.

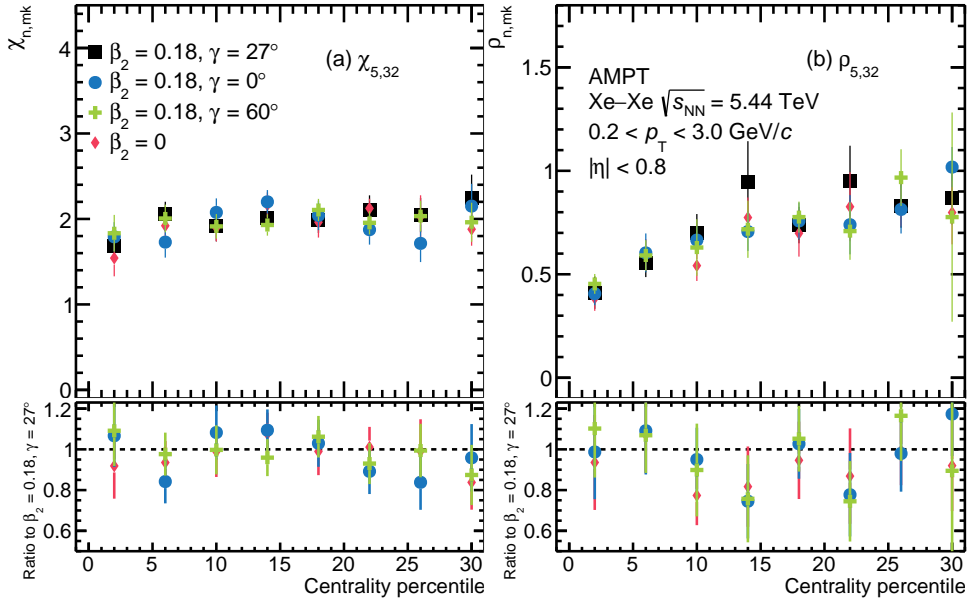


Fig. 15. Centrality dependence of nonlinear modes including (a) $\chi_{5,32}$ and (b) $\rho_{5,32}$ in Xe–Xe collisions at $\sqrt{s_{\text{NN}}} = 5.44$ TeV in AMPT.

7.2 nuclear diffuseness

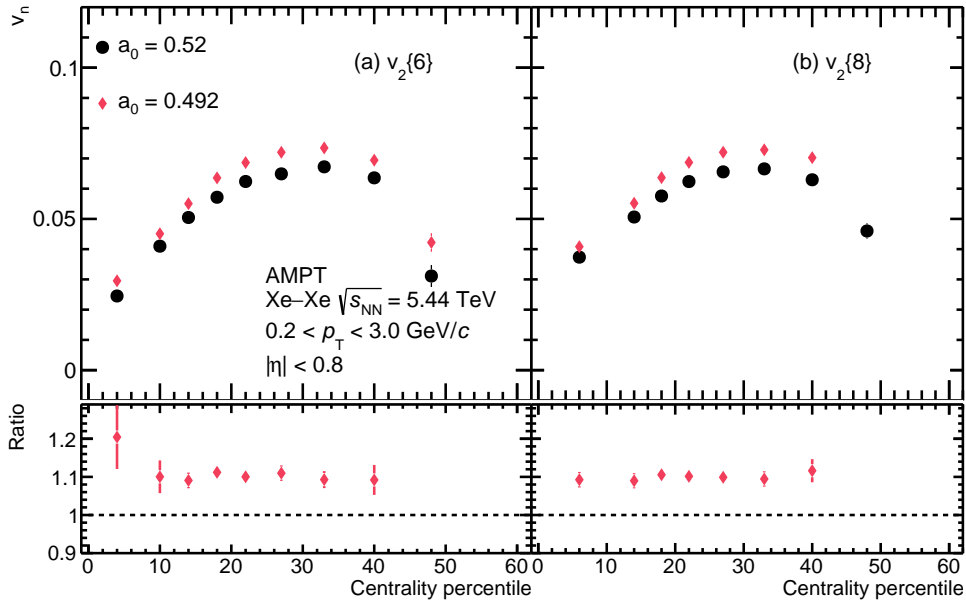


Fig. 16. Centrality dependence of $v_2\{6\}, v_2\{8\}$ in Xe–Xe collisions at $\sqrt{s_{NN}} = 5.44$ TeV in AMPT.

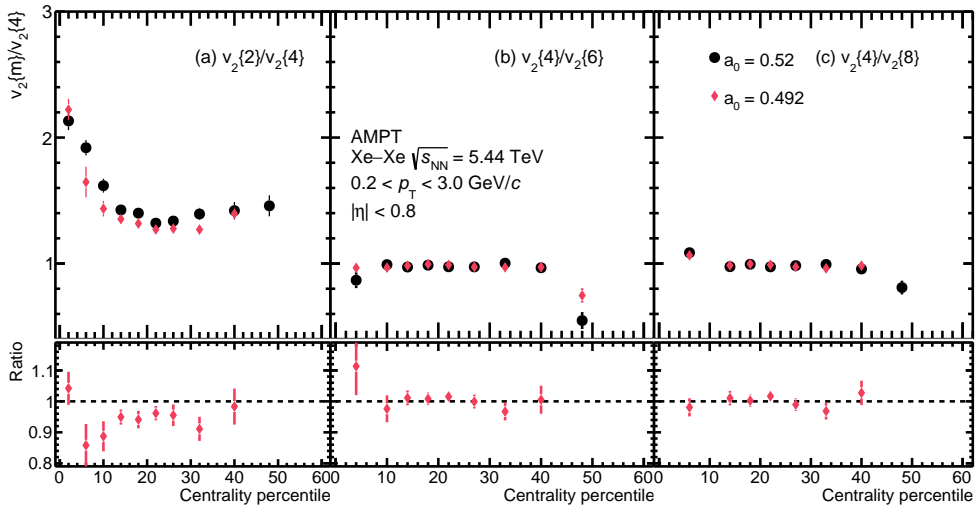


Fig. 17. Centrality dependence of $v_2\{2\}/v_2\{4\}, v_2\{6\}/v_2\{4\}, v_2\{8\}/v_2\{4\}$ in Xe–Xe collisions at $\sqrt{s_{NN}} = 5.44$ TeV in AMPT.

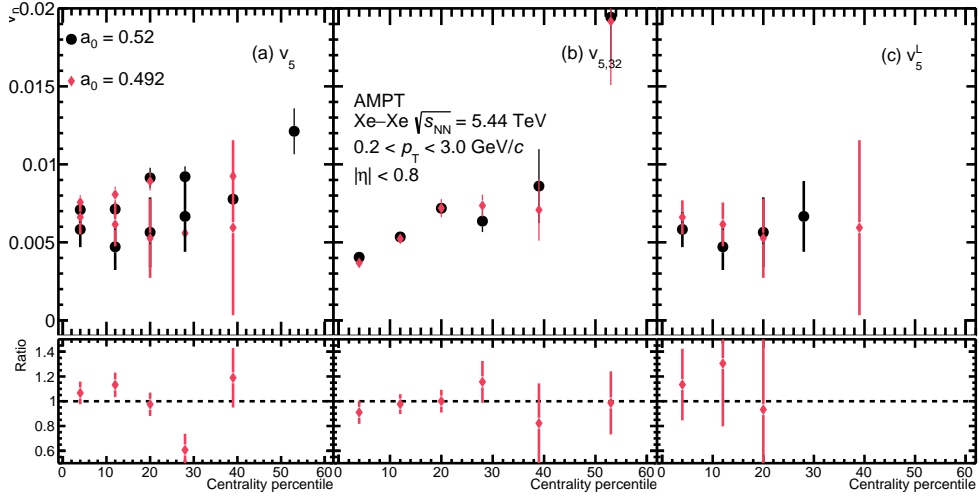


Fig. 18. Centrality dependence of nonlinear modes including (a) v_4 , (b) $v_{4,22}$ and (c) Linear v_4 in Xe–Xe collisions at $\sqrt{s_{NN}} = 5.44$ TeV in AMPT.

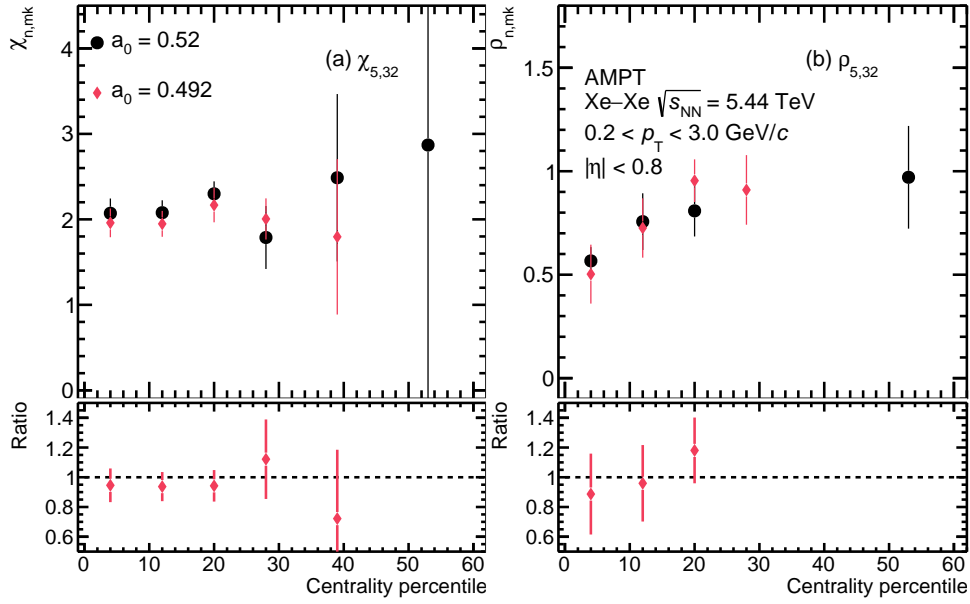


Fig. 19. Centrality dependence of nonlinear modes including (a) $\chi_{5,32}$ and (b) $\rho_{5,32}$ in Xe–Xe collisions at $\sqrt{s_{NN}} = 5.44$ TeV in AMPT.

References

1. E. V. Shuryak, “Quantum Chromodynamics and the Theory of Superdense Matter,” *Phys. Rept.* **61** (1980) 71–158.
2. E. V. Shuryak, “Quark-Gluon Plasma and Hadronic Production of Leptons, Photons and Psions,” *Phys. Lett. B* **78** (1978) 150.

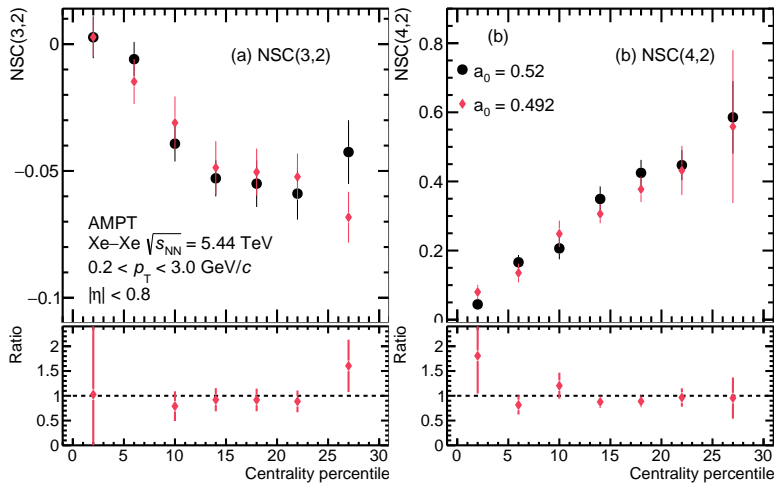


Fig. 20. Centrality dependence of $NSC(m, n)$ in Xe–Xe collisions at $\sqrt{s_{NN}} = 5.44$ TeV in AMPT.

3. R. A. Lacey, N. N. Ajitanand, J. M. Alexander, P. Chung, W. G. Holzmann, M. Issah, A. Taranenko, P. Danielewicz, and H. Stoecker, “Has the QCD Critical Point been Signaled by Observations at RHIC?,” *Phys. Rev. Lett.* **98** (2007) 092301, [arXiv:nucl-ex/0609025](#).
4. D. Molnar and P. Huovinen, “Dissipative effects from transport and viscous hydrodynamics,” *J. Phys. G* **35** (2008) 104125, [arXiv:0806.1367 \[nucl-th\]](#).
5. B. Muller, J. Schukraft, and B. Wyslouch, “First Results from Pb+Pb collisions at the LHC,” *Ann. Rev. Nucl. Part. Sci.* **62** (2012) 361–386, [arXiv:1202.3233 \[hep-ex\]](#).
6. H.-J. Drescher, A. Dumitru, C. Gombeaud, and J.-Y. Ollitrault, “The Centrality dependence of elliptic flow, the hydrodynamic limit, and the viscosity of hot QCD,” *Phys. Rev. C* **76** (2007) 024905, [arXiv:0704.3553 \[nucl-th\]](#).
7. U. Heinz and R. Snellings, “Collective flow and viscosity in relativistic heavy-ion collisions,” *Ann. Rev. Nucl. Part. Sci.* **63** (2013) 123–151, [arXiv:1301.2826 \[nucl-th\]](#).
8. D. Molnar and M. Gyulassy, “Saturation of elliptic flow and the transport opacity of the gluon plasma at RHIC,” *Nucl. Phys. A* **697** (2002) 495–520, [arXiv:nucl-th/0104073](#). [Erratum: *Nucl. Phys. A* 703, 893–894 (2002)].
9. H. Song, Y. Zhou, and K. Gajdosova, “Collective flow and hydrodynamics in large and small systems at the LHC,” *Nucl. Sci. Tech.* **28** no. 7, (2017) 99, [arXiv:1703.00670 \[nucl-th\]](#).
10. D. Teaney, “The Effects of viscosity on spectra, elliptic flow, and HBT radii,” *Phys. Rev. C* **68** (2003) 034913, [arXiv:nucl-th/0301099](#).
11. Z. Xu, C. Greiner, and H. Stoecker, “PQCD calculations of elliptic flow and shear viscosity at RHIC,” *Phys. Rev. Lett.* **101** (2008) 082302, [arXiv:0711.0961 \[nucl-th\]](#).
12. S. Voloshin and Y. Zhang, “Flow study in relativistic nuclear collisions by Fourier expansion of Azimuthal particle distributions,” *Z. Phys. C* **70** (1996) 665–672, [arXiv:hep-ph/9407282](#).
13. H. Niemi, G. S. Denicol, H. Holopainen, and P. Huovinen, “Event-by-event distributions of azimuthal asymmetries in ultrarelativistic heavy-ion collisions,” *Phys. Rev. C* **87** no. 5, (2013) 054901, [arXiv:1212.1008 \[nucl-th\]](#).

14. A. Bilandzic, C. H. Christensen, K. Gulbrandsen, A. Hansen, and Y. Zhou, “Generic framework for anisotropic flow analyses with multiparticle azimuthal correlations,” *Phys. Rev. C* **89** no. 6, (2014) 064904, [arXiv:1312.3572](#) [nucl-ex].
15. ATLAS Collaboration, G. Aad *et al.*, “Measurement of the correlation between flow harmonics of different order in lead-lead collisions at $\sqrt{s_{NN}}=2.76$ TeV with the ATLAS detector,” *Phys. Rev. C* **92** no. 3, (2015) 034903, [arXiv:1504.01289](#) [hep-ex].
16. J. Qian and U. Heinz, “Hydrodynamic flow amplitude correlations in event-by-event fluctuating heavy-ion collisions,” *Phys. Rev. C* **94** no. 2, (2016) 024910, [arXiv:1607.01732](#) [nucl-th].
17. X. Zhu, Y. Zhou, H. Xu, and H. Song, “Correlations of flow harmonics in 2.76A TeV Pb–Pb collisions,” *Phys. Rev. C* **95** no. 4, (2017) 044902, [arXiv:1608.05305](#) [nucl-th].
18. J. E. Bernhard, J. S. Moreland, and S. A. Bass, “Bayesian estimation of the specific shear and bulk viscosity of quark–gluon plasma,” *Nature Phys.* **15** no. 11, (2019) 1113–1117.
19. JETSCAPE Collaboration, D. Everett *et al.*, “Multisystem Bayesian constraints on the transport coefficients of QCD matter,” *Phys. Rev. C* **103** no. 5, (2021) 054904, [arXiv:2011.01430](#) [hep-ph].
20. G. Nijs, W. van der Schee, U. Gürsoy, and R. Snellings, “Transverse Momentum Differential Global Analysis of Heavy-Ion Collisions,” *Phys. Rev. Lett.* **126** no. 20, (2021) 202301, [arXiv:2010.15130](#) [nucl-th].
21. J. E. Parkkila, A. Onnerstad, and D. J. Kim, “Bayesian estimation of the specific shear and bulk viscosity of the quark-gluon plasma with additional flow harmonic observables,” *Phys. Rev. C* **104** no. 5, (2021) 054904, [arXiv:2106.05019](#) [hep-ph].
22. J. Jia, “Shape of atomic nuclei in heavy ion collisions,” *Phys. Rev. C* **105** no. 1, (2022) 014905, [arXiv:2106.08768](#) [nucl-th].
23. C. Zhang and J. Jia, “Evidence of Quadrupole and Octupole Deformations in Zr96+Zr96 and Ru96+Ru96 Collisions at Ultrarelativistic Energies,” *Phys. Rev. Lett.* **128** no. 2, (2022) 022301, [arXiv:2109.01631](#) [nucl-th].
24. G. Giacalone, J. Jia, and C. Zhang, “Impact of nuclear deformation on relativistic heavy-ion collisions: Assessing consistency in nuclear physics across energy scales,” <https://link.aps.org/doi/10.1103/PhysRevLett.127.242301>.
25. J. Jia, G. Giacalone, and C. Zhang, “Separating the impact of nuclear skin and nuclear deformation on elliptic flow and its fluctuations in high-energy isobar collisions,” [arXiv:2206.10449](#) [nucl-th].
26. N. Magdy, “Impact of nuclear deformation on collective flow observables in relativistic U+U collisions,” *Eur. Phys. J. A* **59** no. 3, (2023) 64, [arXiv:2206.05332](#) [nucl-th].
27. J. Jia, G. Giacalone, and C. Zhang, “Precision Tests of the Nonlinear Mode Coupling of Anisotropic Flow via High-Energy Collisions of Isobars,” *Chin. Phys. Lett.* **40** no. 4, (2023) 042501, [arXiv:2206.07184](#) [nucl-th].
28. H.-j. Xu, W. Zhao, H. Li, Y. Zhou, L.-W. Chen, and F. Wang, “Probing nuclear structure with mean transverse momentum in relativistic isobar collisions,” [arXiv:2111.14812](#) [nucl-th].
29. J. Jia, “Probing triaxial deformation of atomic nuclei in high-energy heavy ion collisions,” *Phys. Rev. C* **105** no. 4, (2022) 044905, [arXiv:2109.00604](#) [nucl-th].
30. ALICE Collaboration, “Centrality determination using the Glauber model in Xe-Xe collisions at $\sqrt{s_{NN}} = 5.44$ TeV,”

31. K. Tsukada *et al.*, “First elastic electron scattering from ^{132}Xe at the SCRIT facility,” *Phys. Rev. Lett.* **118** no. 26, (2017) 262501, [arXiv:1703.04278](#) [nucl-ex].
32. W. Fischer *et al.*, “Isotope shifts in the atomic spectrum of xenon and nuclear deformation effects,” *Zeitschrift für Physik* **270** (1974) 113–120.
33. K. Kumar, “Intrinsic Quadrupole Moments and Shapes of Nuclear Ground States and Excited States,” *Phys. Rev. Lett.* **28** (1972) 249–253.
34. A. Poves, F. Nowacki, and Y. Alhassid, “Limits on assigning a shape to a nucleus,” *Phys. Rev. C* **101** no. 5, (2020) 054307, [arXiv:1906.07542](#) [nucl-th].
35. D. Cline, “Nuclear shapes studied by coulomb excitation,” *Ann. Rev. Nucl. Part. Sci.* **36** (1986) 683–716.
36. L. Morrison *et al.*, “Quadrupole deformation of ^{130}Xe measured in a Coulomb-excitation experiment,” *Phys. Rev. C* **102** no. 5, (2020) 054304.
37. ALICE Collaboration, S. Acharya *et al.*, “Anisotropic flow in Xe-Xe collisions at $\sqrt{s_{NN}} = 5.44$ TeV,” *Phys. Lett. B* **784** (2018) 82–95, [arXiv:1805.01832](#) [nucl-ex].
38. ALICE Collaboration, S. Acharya *et al.*, “Characterizing the initial conditions of heavy-ion collisions at the LHC with mean transverse momentum and anisotropic flow correlations,” *Phys. Lett. B* **834** (2022) 137393, [arXiv:2111.06106](#) [nucl-ex].
39. Z.-W. Lin, C. M. Ko, B.-A. Li, B. Zhang, and S. Pal, “A Multi-phase transport model for relativistic heavy ion collisions,” *Phys. Rev. C* **72** (2005) 064901, [arXiv:nucl-th/0411110](#).
40. P. P. Bhaduri and S. Chattopadhyay, “Differential elliptic flow of identified hadrons and constituent quark number scaling at FAIR,” *Phys. Rev. C* **81** (2010) 034906, [arXiv:1002.4100](#) [hep-ph].
41. Y. Guo, S. Shi, S. Feng, and J. Liao, “Magnetic Field Induced Polarization Difference between Hyperons and Anti-hyperons,” *Phys. Lett. B* **798** (2019) 134929, [arXiv:1905.12613](#) [nucl-th].
42. M. R. Haque, M. Nasim, and B. Mohanty, “Systematic investigation of azimuthal anisotropy in Au+Au and U+U collisions at $\sqrt{s_{NN}} = 200$ GeV,” *J. Phys. G* **46** no. 8, (2019) 085104.
43. G.-L. Ma and Z.-W. Lin, “Predictions for $\sqrt{s_{NN}} = 5.02$ TeV Pb+Pb Collisions from a Multi-Phase Transport Model,” *Phys. Rev. C* **93** no. 5, (2016) 054911, [arXiv:1601.08160](#) [nucl-th].
44. N. Magdy, O. Evdokimov, and R. A. Lacey, “A method to test the coupling strength of the linear and nonlinear contributions to higher-order flow harmonics via Event Shape Engineering,” *J. Phys. G* **48** no. 2, (2020) 025101, [arXiv:2002.04583](#) [nucl-ex].
45. M. Nasim, L. Kumar, P. K. Netrakanti, and B. Mohanty, “Energy dependence of elliptic flow from heavy-ion collision models,” *Phys. Rev. C* **82** (2010) 054908, [arXiv:1010.5196](#) [nucl-ex].
46. J. Xu and C. M. Ko, “The effect of triangular flow on di-hadron azimuthal correlations in relativistic heavy ion collisions,” *Phys. Rev. C* **83** (2011) 021903, [arXiv:1011.3750](#) [nucl-th].
47. J. Xu and C. M. Ko, “Triangular flow in heavy ion collisions in a multiphase transport model,” *Phys. Rev. C* **84** (2011) 014903, [arXiv:1103.5187](#) [nucl-th].
48. X.-N. Wang and M. Gyulassy, “Energy and centrality dependence of rapidity densities at RHIC,” *Phys. Rev. Lett.* **86** (2001) 3496–3499, [arXiv:nucl-th/0008014](#).

49. B. Zhang, “ZPC 1.0.1: A Parton cascade for ultrarelativistic heavy ion collisions,” *Comput. Phys. Commun.* **109** (1998) 193–206, [arXiv:nucl-th/9709009](#).
50. L.-W. Chen and C. M. Ko, “System size dependence of elliptic flows in relativistic heavy-ion collisions,” *Phys. Lett. B* **634** (2006) 205–209, [arXiv:nucl-th/0505044](#).
51. B.-A. Li and C. M. Ko, “Formation of superdense hadronic matter in high-energy heavy ion collisions,” *Phys. Rev. C* **52** (1995) 2037–2063, [arXiv:nucl-th/9505016](#).
52. B. Bally, M. Bender, G. Giacalone, and V. Somà, “Evidence of the triaxial structure of ^{129}Xe at the Large Hadron Collider,” *Phys. Rev. Lett.* **128** no. 8, (2022) 082301, [arXiv:2108.09578 \[nucl-th\]](#).
53. G.-L. Ma and A. Bzdak, “Long-range azimuthal correlations in proton–proton and proton–nucleus collisions from the incoherent scattering of partons,” *Phys. Lett. B* **739** (2014) 209–213, [arXiv:1404.4129 \[hep-ph\]](#).
54. A. Bzdak and G.-L. Ma, “Elliptic and triangular flow in $p+\text{Pb}$ and peripheral $\text{Pb}+\text{Pb}$ collisions from parton scatterings,” *Phys. Rev. Lett.* **113** no. 25, (2014) 252301, [arXiv:1406.2804 \[hep-ph\]](#).
55. Z. Feng, G.-M. Huang, and F. Liu, “Anisotropic flow of $\text{Pb}+\text{Pb}$ $\sqrt{s_{\text{NN}}} = 5.02$ TeV from a Multi-Phase Transport Model,” *Chin. Phys. C* **41** no. 2, (2017) 024001, [arXiv:1606.02416 \[nucl-ex\]](#).
56. A. Bilandzic, R. Snellings, and S. Voloshin, “Flow analysis with cumulants: Direct calculations,” *Phys. Rev. C* **83** (2011) 044913, [arXiv:1010.0233 \[nucl-ex\]](#).
57. N. Borghini, P. M. Dinh, and J.-Y. Ollitrault, “A New method for measuring azimuthal distributions in nucleus-nucleus collisions,” *Phys. Rev. C* **63** (2001) 054906, [arXiv:nucl-th/0007063](#).
58. Z. Moravcova, K. Gulbrandsen, and Y. Zhou, “Generic algorithm for multiparticle cumulants of azimuthal correlations in high energy nucleus collisions,” *Phys. Rev. C* **103** no. 2, (2021) 024913, [arXiv:2005.07974 \[nucl-th\]](#).
59. S. A. Voloshin, A. M. Poskanzer, A. Tang, and G. Wang, “Elliptic flow in the Gaussian model of eccentricity fluctuations,” *Phys. Lett. B* **659** (2008) 537–541, [arXiv:0708.0800 \[nucl-th\]](#).
60. H. Song, S. A. Bass, U. Heinz, T. Hirano, and C. Shen, “200 A GeV Au+Au collisions serve a nearly perfect quark-gluon liquid,” *Phys. Rev. Lett.* **106** (2011) 192301, [arXiv:1011.2783 \[nucl-th\]](#). [Erratum: *Phys.Rev.Lett.* 109, 139904 (2012)].
61. R. S. Bhalerao, J.-Y. Ollitrault, and S. Pal, “Characterizing flow fluctuations with moments,” *Phys. Lett. B* **742** (2015) 94–98, [arXiv:1411.5160 \[nucl-th\]](#).
62. R. S. Bhalerao, J.-Y. Ollitrault, and S. Pal, “Event-plane correlators,” *Phys. Rev. C* **88** (2013) 024909, [arXiv:1307.0980 \[nucl-th\]](#).
63. L. Yan and J.-Y. Ollitrault, “ $\nu_4, \nu_5, \nu_6, \nu_7$: nonlinear hydrodynamic response versus LHC data,” *Phys. Lett. B* **744** (2015) 82–87, [arXiv:1502.02502 \[nucl-th\]](#).
64. **ALICE** Collaboration, S. Acharya *et al.*, “Linear and non-linear flow modes in Pb-Pb collisions at $\sqrt{s_{\text{NN}}} = 2.76$ TeV,” *Phys. Lett. B* **773** (2017) 68–80, [arXiv:1705.04377 \[nucl-ex\]](#).
65. Y. Zhou, K. Xiao, Z. Feng, F. Liu, and R. Snellings, “Anisotropic distributions in a multiphase transport model,” *Phys. Rev. C* **93** no. 3, (2016) 034909, [arXiv:1508.03306 \[nucl-ex\]](#).
66. P. Huo, K. Gajdošová, J. Jia, and Y. Zhou, “Importance of non-flow in mixed-harmonic multi-particle correlations in small collision systems,” *Phys.*

- Lett. B* **777** (2018) 201–206, [arXiv:1710.07567](#) [nucl-ex].
67. H. Niemi, K. J. Eskola, and R. Paatelainen, “Event-by-event fluctuations in a perturbative QCD + saturation + hydrodynamics model: Determining QCD matter shear viscosity in ultrarelativistic heavy-ion collisions,” *Phys. Rev. C* **93** no. 2, (2016) 024907, [arXiv:1505.02677](#) [hep-ph].
 68. B. Schenke, C. Shen, and D. Teaney, “Transverse momentum fluctuations and their correlation with elliptic flow in nuclear collision,” *Phys. Rev. C* **102** no. 3, (2020) 034905, [arXiv:2004.00690](#) [nucl-th].
 69. **ALICE** Collaboration, S. Acharya *et al.*, “Energy dependence and fluctuations of anisotropic flow in Pb-Pb collisions at $\sqrt{s_{NN}} = 5.02$ and 2.76 TeV,” *JHEP* **07** (2018) 103, [arXiv:1804.02944](#) [nucl-ex].
 70. **ALICE** Collaboration, S. Acharya *et al.*, “Higher harmonic non-linear flow modes of charged hadrons in Pb-Pb collisions at $\sqrt{s_{NN}} = 5.02$ TeV,” *JHEP* **05** (2020) 085, [arXiv:2002.00633](#) [nucl-ex].
 71. S. Zhao, H.-j. Xu, Y.-X. Liu, and H. Song, “Probing the nuclear deformation with three-particle asymmetric cumulant in RHIC isobar runs,” *Phys. Lett. B* **839** (2023) 137838, [arXiv:2204.02387](#) [nucl-th].
 72. **ALICE** Collaboration, J. Adam *et al.*, “Correlated event-by-event fluctuations of flow harmonics in Pb-Pb collisions at $\sqrt{s_{NN}} = 2.76$ TeV,” *Phys. Rev. Lett.* **117** (2016) 182301, [arXiv:1604.07663](#) [nucl-ex].
 73. **ALICE** Collaboration, S. Acharya *et al.*, “Measurements of mixed harmonic cumulants in Pb-Pb collisions at $\sqrt{s_{NN}} = 5.02$ TeV,” *Phys. Lett. B* **818** (2021) 136354, [arXiv:2102.12180](#) [nucl-ex].
 74. **ALICE** Collaboration, S. Acharya *et al.*, “Systematic studies of correlations between different order flow harmonics in Pb-Pb collisions at $\sqrt{s_{NN}} = 2.76$ TeV,” *Phys. Rev. C* **97** no. 2, (2018) 024906, [arXiv:1709.01127](#) [nucl-ex].